

Large-scale multilayer architecture of single-atom arrays with individual addressability

Malte Schlosser, Sascha Tichelmann, Dominik Schäffner, Daniel Ohl de Mello, Moritz Hambach, and Gerhard Birk^{1*}

Institut für Angewandte Physik, Technische Universität Darmstadt,

Schlossgartenstraße 7, 64289 Darmstadt, Germany

(Dated: December 15, 2024)

We report on the realization of a novel platform for the creation of large-scale 3D multilayer configurations of planar arrays of individual neutral atoms: a microlens-generated Talbot optical lattice. We demonstrate the trapping and imaging of rubidium atoms in integer and fractional Talbot planes and realize the in-plane assembly of defect-free atom arrays. We present interleaved lattices with dynamic position control and parallelized sub-lattice addressing of spin states. The single beam illumination of a microlens array constitutes a structurally robust and wavelength-universal method for the realization of 3D atomic arrays with favourable scaling properties due to the inherent self-imaging of the focal array. Geometry and trap size are configurable in the micrometer regime with immediate applications in quantum science and technology.

Outstanding progress in atomic physics has paved the way for experiments which probe and exploit the laws of quantum mechanics at the single quantum level [1, 2]. A cornerstone are neutral atoms trapped by light [3], which constitute a versatile experimental platform where internal and external degrees of freedom can be coherently manipulated and interactions are dynamically tunable. This comprehensive control is the key element of forefront research in an extensive field including quantum chemistry [4, 5], quantum interferometry [6], quantum metrology [7, 8], quantum information processing [9, 10] and quantum simulation [11, 12].

A natural focus are multi-site geometries created by optical lattices [13–16] and arrays of optical tweezers [17–28]. The former can serve as carrier for large numbers of isolated probes, thereby taintlessly boosting signal and sensitivity, as well as they can provide many-body systems with defined atom number per site and controllable tunnelling. Fostered by quantum gas microscopes with access to local observables, the top-down implementation of condensed matter models [14, 15] and the realization of record optical clocks [29] has been demonstrated.

Flexible arrays of optical tweezers created by focused laser beams decouple trap size and separation as well as array geometry from the constraint of interference, which is imposed on optical lattices. Their inherently resolved trapping sites are adaptable to either hold a bulk of atoms [30, 31], number resolved ensembles [32, 33], or single atoms [34, 35] and can be composed from multiple colours of laserlight [5, 18, 36]. Straightforward dynamic position control represents a fruitful tool which facilitates the coherent transport of quantum states [37, 38] and the seminal assembly of defect free sub-arrays [19–21, 25, 27]. Thus, arrays of individually controlled microtraps lend themselves to the bottom-up engineering of quantum systems with configurable tunnel-coupling [39–41] and on-demand Rydberg interactions [9, 10, 42]. Pioneering implementations realized the fundamental building blocks of the Bose-Hubbard [39] and the Hubbard model [40], the formation of a molecule [5] and small spin systems

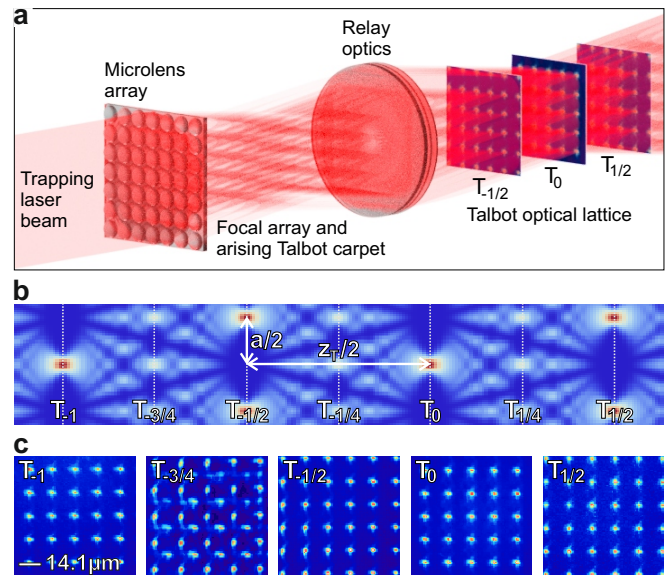


FIG. 1. (color online) Microlens-array generated Talbot optical lattice. (a) Simplified schematic of the experimental setup. The 2D periodic spot pattern of the focal plane gives rise to the formation of a 3D Talbot carpet. After reimaging and demagnification, we obtain a site-resolved multilayer lattice of 2D periodic microtrap arrays formed from regular self-images of the generating focal plane (for clarity, only three planes are drawn). (b) Detail of the Talbot carpet created by an array of Gaussian beams with parameters according to the experiment (2D projection). (c) Averaged fluorescence of single atoms stored in the trap arrays of integer and fractional Talbot planes (see text for details).

with Rydberg interactions ranging from dynamically coupled to blockaded [19, 20, 42].

For future progress, scalability is pivotal. In this article, we address this evident need for a configurable large scale implementation with a novel platform, as depicted in Fig. 1. We harness the Talbot effect [43, 44] to multiply a microlens-array (MLA) generated 2D periodic configuration of single-atom microtraps to a multilayer architecture in the third dimension. This Talbot optical lattice

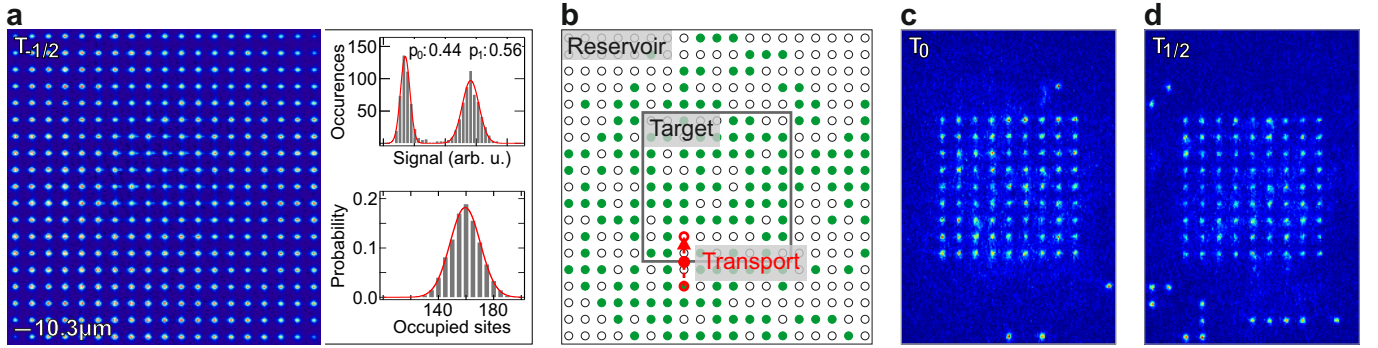


FIG. 2. (color online) Micro-optical realization of a Talbot optical lattice with more than 400 sites per principal plane and in-plane assembly of a defect-free 9×9 cluster. (a) 19×19 site detail showing the averaged fluorescence at the resolved trapping positions (left), and histograms of the detected fluorescence at a single site (right, top) and the total atom number per realization (right, bottom). The fidelity for the detection of a single atom is $F > 0.99$ and on average 161 sites are loaded with an atom. (b) Initial occupancy matrix of the 19×19 reservoir array with visualized target cluster and atom transport by a superposed moveable optical tweezer (red dot). Occupied (empty) traps are depicted as green dots (gray circles). The assembly process involves multiple cycles of atom rearrangement and position detection [25]. (c, d) In-situ fluorescence of the atom distribution after successful assembly in the lattice plane T_0 and $T_{1/2}$. The trap arrays are centered in the images.

[45, 46] exhibits excellent scalability as it is built in parallel from a microfabricated source element with thousands of lenslets and the self imaging effect which comes at no additional cost.

Figure 1a visualizes the experimental platform: The source element is a quadratic grid MLA of 166×166 refractive lenslets with a pitch of $30.0(3) \mu\text{m}$. A subset of lenslets is illuminated by the Gaussian trapping laser beam with a beam waist of $200(2) \mu\text{m}$ at the position of the MLA and a wavelength of $\lambda = 798.6 \text{ nm}$. The 2D periodic spot pattern in the focal plane is the origin of a 3D Talbot carpet, which exhibits integer and fractional self-images of the generating array – Talbot planes – in the axial dimension. The separation of regular self-images is given by the Talbot length $z_T = 2a^2/\lambda$, which is a function of the spatial period a of the generating array. Fractional self-images are found at fractional multiples of z_T and individual planes T are labeled according to their axial position normalized to z_T with T_0 (focal plane) being the generating array. In our setup, the focal array is reimaged and demagnified by the use of relay optics, which renders the pitch and the associated Talbot length configurable. A noticeable modification due to reimaging is the appearance of negative indexed Talbot planes which complete the symmetric 3D structure of the resulting Talbot optical lattice. In this realization, we have used a generating array with configured pitch of $a = 14.1(4) \mu\text{m}$ and trap waist of $w_0 = 1.45(10) \mu\text{m}$. The Talbot distance evaluates to $z_T = 497(28) \mu\text{m}$. This corresponds to an axial separation of $z_T/2 = 248(14) \mu\text{m}$ for the trap arrays of the principal planes $T_0, T_{\pm 1/2}, T_{\pm 1}, \dots$ which reproduce the same in-plane geometry. Figure 1b shows a 2D projection of the Talbot carpet which covers the planes T_{-1} to $T_{1/2}$ along the optical axis.

We superimpose a standard magneto-optical trap and

load the lattice sites with laser-cooled ^{85}Rb atoms during a sequence of optical molasses. Typical trap depths are on the order of $k_B \cdot 1 \text{ mK}$. For the preparation of an atomic 2D Talbot register, the imaging system is focused to the selected plane and the atoms in all other planes are removed with a resonant blow-away laser. Figure 1c exemplarily shows the averaged fluorescence of single atoms stored in the focal plane T_0 and in the Talbot planes $T_{-1}, T_{-3/4}$ and $T_{\pm 1/2}$. The trap positions are stable and optically resolved which reveals the underlying periodic geometry. In contrast to the principal planes, for the fractional plane $T_{-3/4}$ the number of trapping sites with visible atomic fluorescence differs from a simple model. As expected, the trap pitch is reduced by a factor of two, but the signal is weaker and even vanishes for a subclass of sites at regular positions. We contribute this behaviour to a modulation of trap depths, which arises from interference effects of light transmitted by the lenslets and light transmitted through the interspaces of the MLA as well as from components of the light field produced by the spherical shape and limited aperture of the lenslets that are not included in a simple paraxial description [44, 47]. Each 2D layer can serve as a single atom quantum register with a readily scalable number of sites. For the experimental implementation presented in Fig. 2, we use a modified setup based on a different MLA with more than 400 optical microtraps per principal plane. We utilize a trapping laser beam of wavelength 796.3 nm with waist of $1923(21) \mu\text{m}$ and a quadratic grid MLA with a pitch of $110.0(3) \mu\text{m}$. The trap pitch of the principal lattice planes is configured to $10.3(3) \mu\text{m}$ and the traps have a waist of $1.45(10) \mu\text{m}$. The Talbot length is $z_T = 267(15) \mu\text{m}$. Figure 2a gives an averaged fluorescence image of a 19×19 site detail of the plane $T_{-1/2}$. The preparation process based on light assisted collisions

results in a heavily sub-Poissonian distribution stemming from the effect of collisional blockade [34]. The histogram of the fluorescence recorded for a single site (top) exhibits two distinct peaks corresponding to background light and the fluorescence of a single atom. A Gaussian fit to the data yields the probabilities for no-atom (p_0) and one-atom (p_1) events as given in the graph. We do not observe any two-atom events. On average 161 sites are loaded with an atom, as obtained from the binomial fit to the histogram of the number of occupied sites (bottom). Values of $p_1 > 0.5$ indicate the presence of two-body collisional events which cause only one of the participants (instead of both) to leave the trap. This channel allows for the near-deterministic preparation of single atoms [27, 35].

The stochastic nature of the loading process leads to random atomic positions, whereas a broad range of applications pre-requires defect-free atomic arrays and the ability to mend atom loss during operation. This necessitates the incorporation of techniques for individual atom transport and deterministic target pattern assembly [19–21, 25, 27, 37, 38, 48]. For this purpose, we use a superposed moveable auxiliary laser beam, which acts as an optical tweezer. This technique is applicable to any plane of the lattice in a straight-forward fashion. In our setup, the tweezer is aligned with the imaging system and therefore automatically focused to the selected lattice plane. Figure 2b visualizes the principle of operation, which is detailed in [25], where it has been applied for the rearrangement of atoms in the re-imaged focal plane T_0 . Starting from the initial occupancy matrix, a sequence of transport operations is performed in order to reach complete filling of the target structure and the resulting occupancy is analyzed. The detection of residual defects triggers another rearrangement cycle, which significantly enhances success rates and achievable structure sizes. In the work presented here, we define a 9×9 atomic cluster as target structure and the reservoir grid consists of 19×19 sites. Figures 2c,d show in-situ fluorescence of the atomic pattern after successful assembly in the plane T_0 and $T_{1/2}$.

The single-atom quantum register of a selected plane can be extended to parallelized and interleaved geometries of multiple focused beam arrays by employing multiple MLAs as well as by the illumination of an individual MLA with multiple trapping laser beams. This allows one to dynamically compose quantum registers with flexible site separation from superimposed moveable trap arrays [38].

Figure 3 shows configurations created from two interleaved sub-registers of the Talbot plane $T_{1/2}$ with fundamental pitch of $14.1(4)$ μm . These are implemented by expanding the setup used in the first section with a second trapping laser beam which irradiates the MLA under a modified incident angle, having a waist of $202(2)$ μm and a frequency difference of 30.0 MHz to avoid interferences.

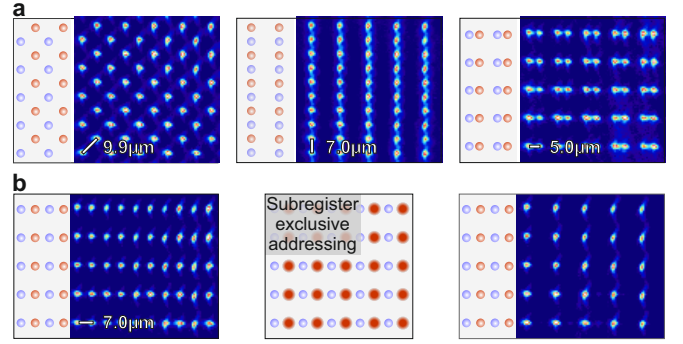


FIG. 3. (color online) Interleaved configuration of two Talbot lattices. All images show averaged fluorescence of the $T_{1/2}$ plane and the presented geometries are visualized by red and blue dots depicting the sites of the two lattices. (a) Single atom registers with tunable atomic separation. The separation of neighbouring traps is (from left to right): $9.9(3)$ μm , $7.0(2)$ μm , and $5.0(2)$ μm . (b) Subregister exclusive addressing of stored atoms is used to convert a spin polarized register ($F = 2$, left) to a configuration of column-wise alternating spin states ($F = 2$ and $F = 3$, right). State-selective detection records fluorescence for atoms in $F = 2$ only.

ence effects. An enclosed angle of 6.3 mrad introduces an offset of half the trap pitch for the respective trap arrays. Figure 3a (left) shows a uniform arrangement that reduces the pitch by a factor of $\sqrt{2}$ and forms a super-register with $9.9(3)$ μm trap separation, with each site of a respective sub-register being equidistant to four sites of the other one. A multitude of atom-chains with $7.0(2)$ μm distance for the atoms within each column is created in Fig. 3a (middle). Furthermore, the trap positions can be tuned to favour pairs of atoms as demonstrated with a separation of $5.0(2)$ μm for neighbouring atoms in Fig. 3a (right). In the current implementation, traps stay independent for a minimum separation of 3 μm which is consistent with the trap waist.

Each of the sub-registers remains independently addressable by selectively illuminating the respective microlenses, which in turn focus the light onto the trapping sites and thereby amplify the atom-light coupling. If the addressing beam is set to spatial overlap with the trapping light it is auto-aligned with the traps while the spacing of interleaved quantum registers can be arbitrarily set within the limits given by trap pitch and trap waist. In the experiments of Fig. 3b we have used this technique for the spin-selective addressing of single atoms stored in sub-registers with a $7.0(2)$ μm spacing. First, all atoms in the complete set of traps are initialized to the $F = 2$ state of the ^{85}Rb ground state hyperfine manifold and state-selectively detected afterwards by removing the population of the $F = 3$ state prior to detection (left). The results displayed on the right account for a modified experimental sequence where laser addressing transfers the atoms to the $F = 3$ state in a sub-register exclusive fashion, resulting in vanishing fluorescence at the addressed

sites. The addressing beam at 795 nm is resonant to the transition $|5S_{1/2}, F = 2\rangle \leftrightarrow |5P_{1/2}, F = 3\rangle$ and is brought to spatial overlap with one of the trapping laser beams by the use of an optical fiber. For the center trap, we obtain $p_1 = 0.47(2)$ before and $p_1 = 0.01(1)$ after the addressing of the stored atoms. For the unaddressed subarray, we observe a reduction of p_1 on the order of 2 %, which we contribute to chromatic aberrations.

A microlens-generated Talbot optical lattice allows for the creation of multi-site 3D trap arrays with customizable structure sizes in the micrometer regime. With the presented work, focused beam microtrap arrays enter a regime which has formerly been accessible only by phase-sensitive standing wave configurations, yet they retain the simplicity and robustness of the optical setup as well as their inherent features of coherent quantum state transport [38] and single-site addressability [49]. The straight-forward assembly of defect-free atomic arrays facilitates bottom-up engineering of quantum systems in microlens generated 2D and 3D trap arrays. In addition, atomic separations can be dynamically adapted in 3D using interleaved configurations, while sub-register exclusive addressability extends techniques for the initialization and read out of quantum states and allows for the parallelization of operations. The implemented Talbot registers provide 161 single-addressable atoms at present with separations well within the limits for coherent Rydberg-mediated interactions with direct implications for neutral atom quantum information processing and quantum simulation architectures [9–11, 50, 51].

We acknowledge financial support from the Deutsche Forschungsgemeinschaft (DFG) through Grant No. BI 647/6-1 within the Priority Program SPP 1929 (GiRyd). We thank the *labscript suite* community and J. Werkmann for support in implementing state-of-the-art control software for our experiments. We thank T. Preuschoff, L. Kohfahl, M.R. Sturm and R. Walser for insightful discussions.

* gerhard.birkl@physik.tu-darmstadt.de; www.iap.tu-darmstadt.de/apq

- [1] S. Haroche, Rev. Mod. Phys. **85**, 1083 (2013).
- [2] D. J. Wineland, Rev. Mod. Phys. **85**, 1103 (2013).
- [3] H. Ott, Reports on Progress in Physics **79**, 054401 (2016).
- [4] G. Qumner and P. S. Julienne, Chemical Reviews **112**, 4949 (2012).
- [5] L. R. Liu, J. D. Hood, Y. Yu, J. T. Zhang, N. R. Hutzler, T. Rosenband, and K.-K. Ni, Science **360**, 900 (2018).
- [6] A. D. Cronin, J. Schmiedmayer, and D. E. Pritchard, Rev. Mod. Phys. **81**, 1051 (2009).
- [7] A. D. Ludlow, M. M. Boyd, J. Ye, E. Peik, and P. O. Schmidt, Rev. Mod. Phys. **87**, 637 (2015).
- [8] C. L. Degen, F. Reinhard, and P. Cappellaro, Rev. Mod. Phys. **89**, 035002 (2017).
- [9] M. Saffman, T. G. Walker, and K. Mølmer, Rev. Mod. Phys. **82**, 2313 (2010).
- [10] M. Saffman, Journal of Physics B: Atomic, Molecular and Optical Physics **49**, 202001 (2016).
- [11] I. M. Georgescu, S. Ashhab, and F. Nori, Rev. Mod. Phys. **86**, 153 (2014).
- [12] J. Argüello-Luengo, A. González-Tudela, T. Shi, P. Zoller, and J. I. Cirac, arXiv preprint arXiv:1807.09228 (2018).
- [13] I. Bloch, J. Dalibard, and S. Nascimbene, Nat Phys **8**, 267 (2012).
- [14] C. Gross and I. Bloch, Science **357**, 995 (2017).
- [15] P. Schauss, Quantum Science and Technology **3**, 023001 (2018).
- [16] A. Kumar, T.-Y. Wu, F. Giraldo, and D. S. Weiss, Nature **561**, 83 (2018).
- [17] M. Schlosser, S. Tichelmann, J. Kruse, and G. Birkl, Quantum Information Processing **10**, 907 (2011).
- [18] M. J. Piotrowicz, M. Lichtman, K. Maller, G. Li, S. Zhang, L. Isenhower, and M. Saffman, Phys. Rev. A **88**, 013420 (2013).
- [19] H. Bernien, S. Schwartz, A. Keesling, H. Levine, A. Omran, H. Pichler, S. Choi, A. S. Zibrov, M. Endres, M. Greiner, *et al.*, Nature **551**, 579 (2017).
- [20] H. Kim, Y. Park, K. Kim, H.-S. Sim, and J. Ahn, Phys. Rev. Lett. **120**, 180502 (2018).
- [21] D. Barredo, V. Lienhard, S. De Léséleuc, T. Lahaye, and A. Browaeys, Nature **561**, 79 (2018).
- [22] C. Sheng, X. He, P. Xu, R. Guo, K. Wang, Z. Xiong, M. Liu, J. Wang, and M. Zhan, Phys. Rev. Lett. **121**, 240501 (2018).
- [23] M. A. Norcia, A. W. Young, and A. M. Kaufman, Phys. Rev. X **8**, 041054 (2018).
- [24] A. Cooper, J. P. Covey, I. S. Madjarov, S. G. Porsev, M. S. Safronova, and M. Endres, Phys. Rev. X **8**, 041055 (2018).
- [25] D. Ohl de Mello, D. Schäffner, J. Werkmann, T. Preuschoff, L. Kohfahl, M. Schlosser, and G. Birkl, arXiv preprint arXiv:1902.00284 (2019).
- [26] S. Saskin, J. Wilson, B. Grinkemeyer, and J. Thompson, arXiv preprint arXiv:1810.10517 (2018).
- [27] M. Brown, T. Thiele, C. Kiehl, T.-W. Hsu, and C. Regal, arXiv preprint arXiv:1811.01448 (2018).
- [28] L. Anderegg, L. W. Cheuk, Y. Bao, S. Burchesky, W. Ketterle, K.-K. Ni, and J. M. Doyle, arXiv preprint arXiv:1902.00497 (2019).
- [29] G. E. Marti, R. B. Hutson, A. Goban, S. L. Campbell, N. Poli, and J. Ye, Phys. Rev. Lett. **120**, 103201 (2018).
- [30] S. J. M. Kuppens, K. L. Corwin, K. W. Miller, T. E. Chupp, and C. E. Wieman, Phys. Rev. A **62**, 013406 (2000).
- [31] R. Dumke, M. Volk, T. Müther, F. B. J. Buchkremer, G. Birkl, and W. Ertmer, Phys. Rev. Lett. **89**, 097903 (2002).
- [32] F. Serwane, G. Zürn, T. Lompe, T. B. Ottenstein, A. N. Wenz, and S. Jochim, Science **332**, 336 (2011).
- [33] M. McGovern, A. J. Hilliard, T. Grünzweig, and M. F. Andersen, Opt. Lett. **36**, 1041 (2011).
- [34] N. Schlosser, G. Reymond, I. Protsenko, and P. Grangier, Nature **411**, 1024 (2001).
- [35] T. Grünzweig, A. Hilliard, M. McGovern, and M. F. Andersen, Nat. Phys. **6**, 951 (2011).
- [36] M. Schlosser, J. Kruse, and G. Birkl, arXiv preprint arXiv:1902.00370 (2019).

- [37] J. Beugnon, C. Tuchendler, H. Marion, A. Gaëtan, Y. Miroshnychenko, Y. R. Sortais, A. M. Lance, M. P. Jones, G. Messin, A. Browaeys, *et al.*, *Nature Physics* **3**, 696 (2007).
- [38] A. Lengwenus, J. Kruse, M. Schlosser, S. Tichelmann, and G. Birk, *Phys. Rev. Lett.* **105**, 170502 (2010).
- [39] A. M. Kaufman, B. J. Lester, C. M. Reynolds, M. L. Wall, M. Foss-Feig, K. R. A. Hazzard, A. M. Rey, and C. A. Regal, *Science* **345**, 306 (2014).
- [40] S. Murmann, A. Bergschneider, V. M. Klinkhamer, G. Zürn, T. Lompe, and S. Jochim, *Phys. Rev. Lett.* **114**, 080402 (2015).
- [41] M. R. Sturm, M. Schlosser, R. Walser, and G. Birk, *Phys. Rev. A* **95**, 063625 (2017).
- [42] A. Browaeys, D. Barredo, and T. Lahaye, *Journal of Physics B: Atomic, Molecular and Optical Physics* **49**, 152001 (2016).
- [43] J. Wen, Y. Zhang, and M. Xiao, *Adv. Opt. Photon.* **5**, 83 (2013).
- [44] B. Besold and N. Lindlein, *Optical Engineering* **36**, 1099 (1997).
- [45] C. Mennerat-Robilliard, D. Boiron, J. M. Fournier, A. Aradian, P. Horak, and G. Grynberg, *EPL (Euro-physics Letters)* **44**, 442 (1998).
- [46] Y. B. Ovchinnikov, *Phys. Rev. A* **73**, 033404 (2006).
- [47] H. Kim, W. Lee, H. Lee, and J. Ahn, *Phys. Rev. A* **91**, 033817 (2015).
- [48] M. Schlosser, J. Kruse, C. Gierl, S. Teichmann, S. Tichelmann, and G. Birk, *New Journal of Physics* **14**, 123034 (2012).
- [49] J. Kruse, C. Gierl, M. Schlosser, and G. Birk, *Phys. Rev. A* **81**, 060308 (2010).
- [50] H. Weimer, M. Muller, I. Lesanovsky, P. Zoller, and H. P. Büchler, *Nat Phys* **6**, 382 (2010).
- [51] A. W. Glaetzle, R. M. van Bijnen, P. Zoller, and W. Lechner, *Nature Communications* **8**, 15813 (2017).